04-09 April 2009

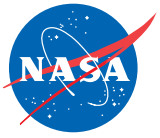

TECH BRIEFS

NATIONAL AERONAUTICS AND SPACE ADMINISTRATION

INTRODUCTION

Tech Briefs are short announcements of innovations originating from research and development activities of the National Aeronautics and Space Administration. They emphasize information considered likely to be transferable across industrial, regional, or disciplinary lines and are issued to encourage commercial application.

Availability of NASA Tech Briefs and TSPs

Requests for individual Tech Briefs or for Technical Support Packages (TSPs) announced herein should be addressed to

National Technology Transfer Center

Telephone No. **(800) 678-6882** or via World Wide Web at **http://www.nttc.edu/about/contactus.asp**

Please reference the control numbers appearing at the end of each Tech Brief. Information on NASA's Innovative Partnerships Program (IPP), its documents, and services is also available at the same facility or on the World Wide Web at **http://ipp.nasa.gov**.

Innovative Partnerships Offices are located at NASA field centers to provide technology-transfer access to industrial users. Inquiries can be made by contacting NASA field centers listed below.

NASA Field Centers and Program Offices

Ames Research Center
Lisa L. Lockyer
(650) 604-1754
lisa.l.lockyer@nasa.gov

Dryden Flight Research Center
Gregory Poteat
(661) 276-3872
greg.poteat@dfrc.nasa.gov

Glenn Research Center
Kathy Needham
(216) 433-2802
kathleen.k.needham@nasa.gov

Goddard Space Flight Center
Nona Cheeks
(301) 286-5810
nona.k.cheeks@nasa.gov

Jet Propulsion Laboratory
Andrew Gray
(818) 354-3821
gray@jpl.nasa.gov

Johnson Space Center
information
(281) 483-3809
jsc.pechtran@mail.nasa.gov

Kennedy Space Center
David R. Makufka
(321) 867-6227
david.r.makufka@nasa.gov

Langley Research Center
Brian Beaton
(757) 864-2192
brian.f.beaton@nasa.gov

Marshall Space Flight Center
Jim Dowdy
(256) 544-7604
jim.dowdy@msfc.nasa.gov

Stennis Space Center
Ramona Travis
(228) 688-3832
ramona.e.travis@nasa.gov

Carl Ray, Program Executive
Small Business Innovation Research (SBIR) & Small Business Technology Transfer (STTR) Programs
(202) 358-4652
carl.g.ray@nasa.gov

Doug Comstock, Director
Innovative Partnerships Program Office
(202) 358-2560
doug.comstock@nasa.gov

04-09 April 2009

TECH BRIEFS

NATIONAL AERONAUTICS AND SPACE ADMINISTRATION

Direct-Solve Image-Based Wavefront Sensing

This method saves time and effort in testing of optical systems.

Goddard Space Flight Center, Greenbelt, Maryland

A method of wavefront sensing (more precisely characterized as a method of determining the deviation of a wavefront from a nominal figure) has been invented as an improved means of assessing the performance of an optical system as affected by such imperfections as misalignments, design errors, and fabrication errors. Unlike some prior methods, this method does not require the use of an expensive, complex interferometric instrument for testing the optical system of interest: indeed, if the system under test includes an image sensor at its focal plane, then this method does not require any optical instrumentation other than the optical system under test. Unlike some other prior methods, this method does not involve processing of multiple defocused images by a nonlinear iterative phase-retrieval algorithm and interpretation of results by a human expert in phase retrieval. Instead, this method involves a single non-iterative algorithm that solves for the wavefront from a single in-focus image, without need for interpretation of results. Hence, the main advantages of this method over the prior methods are reduced computing time and reduced labor.

At the time of writing this article, only fragmentary information about the method is available. Beyond what has been stated above, what is known is the following:

- The method is implemented by software running on a single-processor computer that is connected, via a suitable interface, to the image sensor (typically, a charge-coupled device) in the system under test.
- The software collects a digitized single image from the image sensor.
- The image is displayed on a computer monitor.
- The software directly solves for the wavefront in a time interval of a fraction of a second.
- A picture of the wavefront is displayed.
- The solution process involves, among other things, fast Fourier transforms. It has been reported to the effect that some measure of the wavefront is decomposed into modes of the optical system under test, but it has not been reported whether this decomposition is postprocessing of the solution or part of the solution process.

This work was done by Richard G. Lyon of Goddard Space Flight Center. Further information is contained in a TSP (see page 1). GSC-15208-1

Use of UV Sources for Detection and Identification of Explosives

UV excitation is used to simultaneously detect Raman and fluorescence spectral information of explosive materials.

NASA's Jet Propulsion Laboratory, Pasadena, California

Measurement of Raman and native fluorescence emission using ultraviolet (UV) sources (<400 nm) on targeted materials is suitable for both sensitive detection and accurate identification of explosive materials. When the UV emission data are analyzed using a combination of Principal Component Analysis (PCA) and cluster analysis, chemicals and biological samples can be differentiated based on the geometric arrangement of molecules, the number of repeating aromatic rings, associated functional groups (nitrogen, sulfur, hydroxyl, and methyl), microbial life cycles (spores vs. vegetative cells), and the number of conjugated bonds. Explosive materials can be separated from one another as well as from a range of possible background materials, which includes microbes, car doors, motor oil, and fingerprints on car doors, etc. Many explosives are comprised of similar atomic constituents found in potential background samples such as fingerprint oils/skin, motor oil, and soil. This technique is sensitive to chemical bonds between the elements that lead to the discriminating separability between backgrounds and explosive materials.

The unique combination of the wavelength, optics, mechanical configurations, and chemometrics enables standoff (1 to 5 m) identification of trace amounts of explosive materials with rapid spatial scanning capability. Each data point, which can include both the native fluorescence and Raman signals, is automatically identified in <100 μs by the real-time analysis engine. The rapid acquisition and real-time analysis allows a user to scan the instrument over a large region such that the probability of false negatives resulting from a heterogeneous distribution of explosive material on a surface is dramatically reduced.

The hand-held or robot-mounted instrument has been tested using a number of experimental conditions. In one example, a car panel doped with RDX (an explosive nitroamine) was placed 1 m away from the instrument. The car panel segment was rotated as the instrument collected data to mimic scanning from a fixed distance. The composite traces from the detectors are used by the analysis to show a relatedness index (high values indicate a high match) of each data point as a function of time and spatial position. This sample was part of a blind test to determine whether it was possible to identify RDX on the car panel in the presence of Arizona dust (a standardized interferrant sample). As the sample is scanned, the RDX is found only in specific areas. In the other related experiments where the RDX samples were not so heterogeneous,

the RDX relatedness index was consistently high. In other tests, a limit of detection less than 100 ng/cm^2 was demonstrated at a standoff distance of 1 meter using a 38 mm diameter collection aperture. Using a modestly larger aperture or at higher concentration amounts, the instrument can detect and identify explosives at longer standoff distances.

The developed sensor has an excitation wavelength of 248 nm from a transversely excited hollow cathode (TEHC) laser. An alternate excitation wavelength of interest is 224 nm, also from the TEHC laser. Although the optimum excitation wavelength is less than 250 nm at present, there is also an expectation that longer wavelengths up to about 400 nm may also be relevant for some applications.

This work was done by William Hug and Ray Reid of Photon Systems, Inc., and Rohit Bhartia and Arthur Lane of Caltech for NASA's Jet Propulsion Laboratory under an Army Phase I STTR contract (No. W81XWH-06-C-0395 CM: Dr. Gary Gilbert) with Photon Systems.

In accordance with Public Law 96-517, the contractor has elected to retain title to this invention. Inquiries concerning rights for its commercial use should be addressed to:

Innovative Technology Assets Management
JPL
Mail Stop 202-233
4800 Oak Grove Drive
Pasadena, CA 91109-8099
E-mail: iaoffice@jpl.nasa.gov

Refer to NPO-45166, volume and number of this NASA Tech Briefs *issue, and the page number.*

Using Fluorescent Viruses for Detecting Bacteria in Water

Lyndon B. Johnson Space Center, Houston, Texas

A method of detecting water-borne pathogenic bacteria is based partly on established molecular-recognition and fluorescent-labeling concepts, according to which bacteria of a species of interest are labeled with fluorescent reporter molecules and the bacteria can then be detected by fluorescence spectroscopy. The novelty of the present method lies in the use of bacteriophages (viruses that infect bacteria) to deliver the fluorescent reporter molecules to the bacteria of the species of interest. Bacteriophages that selectively infect that species are selected, and fluorescently labeled virus probes (FLVPs) are prepared by staining these bacteriophages with a fluorescent dye. The FLVPs are immobilized on an optical substrate, which could be a window or a waveguide.

Bacteria/bacteriophage complexes are formed when the substrate is exposed to water containing the bacteria of interest. These complexes exhibit a characteristic fluorescence spectrum, which can be measured to determine the concentration of the complexes and, thus, of the bacteria of interest. Biosensors based on this method could, potentially, enable rapid, selective, and potentially very sensitive detection of bacteria in water. Such biosensors could be used alternatively or complementarily to immunodiagnostic or nucleic acid-based biosensors.

This work was done by Mary Beth Tabacco, Xiaohua Qian, and Jaimie A. Russo of Echo Technologies, Inc., for Johnson Space Center.

In accordance with Public Law 96-517, the contractor has elected to retain title to this invention. Inquiries concerning rights for its commercial use should be addressed to:

Echo Technologies, Inc.
5250 Cherokee Avenue
Alexandria, VA 22312

Refer to MSC-23371-1, volume and number of this NASA Tech Briefs *issue, and the page number.*

Gradiometer Using Middle Loops as Sensing Elements in a Low-Field SQUID MRI System

Device could lead to an MRI diagnostic device for human diagnosis.

NASA's Jet Propulsion Laboratory, Pasadena, California

A new gradiometer scheme uses middle loops as sensing elements in low-field superconducting quantum interference device (SQUID) magnetic resonance imaging (MRI). This design of a second order gradiometer increases its sensitivity and makes it more uniform, compared to the conventional side loop sensing scheme with a comparable matching SQUID. The space between the two middle loops becomes the imaging volume with the enclosing cryostat built accordingly.

For optimal coupling to SQUID, the inductance of the gradiometer must be matched to that of the SQUID input coil. Previously, a second-order gradiometer was designed with optimized wire shape and split middle loops to increase the turn number for increased sensitivity, and/or the size for a larger field of view while keeping the inductance matched. This design was described in "Optimized Geometry for Superconducting Sensing Coils" (NPO-44629), *NASA Tech Briefs*, Vol. 32, No. 1 (January 2008), p. 26.

In a typical configuration of a SQUID MRI, the sensitivity of a gradiometer is a rapidly decreasing function of the distance from the sensing loops. This results in severe non-uniformity of sensitivity and signal-to-noise ratio (SNR) in the image. This problem can be solved by using two second-order gradiometers positioned at the opposite sides of the imaging volume, with two SQUIDs, one per gradiometer. This is not cost-effective since SNR improves only by a square root of two at the center of the imaging volume.

The new design, depicted in the figure, uses a single second-order gradiometer where the middle loops are used for sensing. Both the SNR and the uniformity of the gradiometer are greatly improved. In this scheme, the space between the middle loops be-

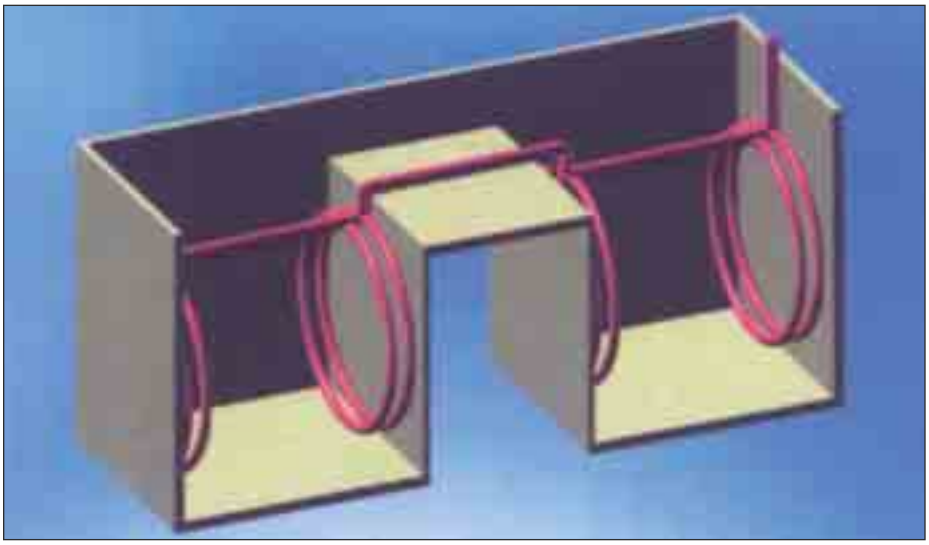

The **Middle-Loop Sensing Gradiometer** concept shows a schematic illustration of cryostat wall geometry (cut-off view). The imaging volume is in between two middle loops, outside the cryostat at room temperature.

comes the imaging volume with the enclosing cryostat built accordingly.

Because of the sensing middle loops at both ends of the imaging volume, the sensitivity at the center of the imaging volume is twice that of conventional geometry with the same SQUID noise. Only about half of the induced energy is lost in the non-sensing loops in the new scheme. The symmetric placement of the sensing loops gives more uniform sensitivity. There is no inductance matching penalty associated with the new configuration, because the geometry and the inductance remain to be that of a single second-order gradiometer.

This work was done by Konstantin Penanen, Inseob Hahn, and Byeong Ho Eom of Caltech for NASA's Jet Propulsion Laboratory. Further information is contained in a TSP (see page 1).

In accordance with Public Law 96-517, the contractor has elected to retain title to this invention. Inquiries concerning rights for its commercial use should be addressed to:

Innovative Technology Assets Management
JPL
Mail Stop 202-233
4800 Oak Grove Drive
Pasadena, CA 91109-8099
E-mail: iaoffice@jpl.nasa.gov

Refer to NPO-45720, volume and number of this NASA Tech Briefs *issue, and the page number.*

Volcano Monitor: Autonomous Triggering of *In-Situ* Sensors

NASA's Jet Propulsion Laboratory, Pasadena, California

In-situ sensors near volcanoes would be alerted by the Earth Observing-1 (EO-1) craft to take more frequent data readings. This project involves developing a sulfur-dioxide-sensing volcano monitor that will be able to transmit its readings through an Iridium modem. The monitor, when integrated into the Sensor Web network, will demonstrate the autonomous capabilities of the Sensor Web, as well as the speed and accuracy of the network. A potential scenario might involve an Earth-based sensor near the volcano, such as a tilt meter or a seismometer, encountering a critical reading. This particular sensor could alert EO-1, which could then look for other sensors in the area. It would then send an alert message down to the Volcano Monitoring Box, which would increase the frequency of its readings from once an hour to once a minute. All these data would then be collected on a Web site that is accessible by volcanologists and other scientists. A typical data reading will include a date, time, temperature reading, humidity reading, and sulfur dioxide reading.

By using the speed and ease with which EO-1 transmits data, information about volcanic activity can be collected quickly and autonomously. In better understanding the volcanoes of Earth, this technology will enable better study and understanding of volcanoes on other moons and planets as NASA sends unmanned vehicles to farther regions of space.

This work was done by Kate Boudreau of University of Idaho, Johanna Cecava of New Mexico State University, and Alberto Behar, Ashley Davies, and Daniel Q. Tran of Caltech for NASA's Jet Propulsion Laboratory. For more information, contact iaoffice@jpl.nasa.gov.
NPO-45445

Wireless Fluid-Level Sensors for Harsh Environments

Sensors can be encased for protection, and are interrogated without wire connections.

Langley Research Center, Hampton, Virginia

Magnetic-field-response sensors have been developed for use in measuring levels of fluids under extreme conditions. The sensors work without wire connections or direct physical contact with power sources, microprocessors, data-acquisition equipment, or electrical circuitry. For fuel-level sensors, the absence of wire connections offers an important safety advantage in elimination of potential ignition sources.

The sensors can be designed for

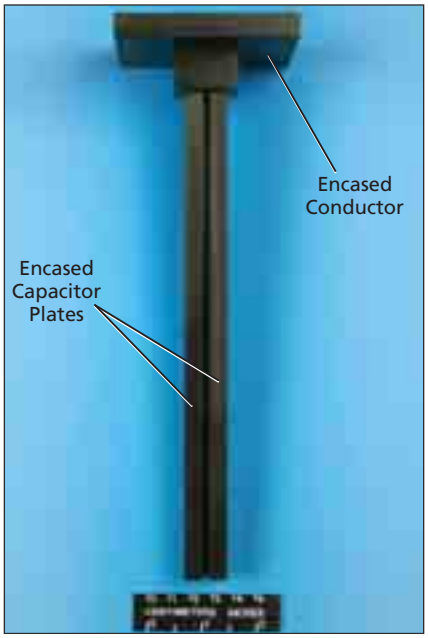

Figure 1. This **Liquid-Level Sensor** comprises two parallel capacitor plates and an inductor, all completely encased in poly(ethylene terephthalate) that has been formulated to afford protection against acids and similar harsh liquids.

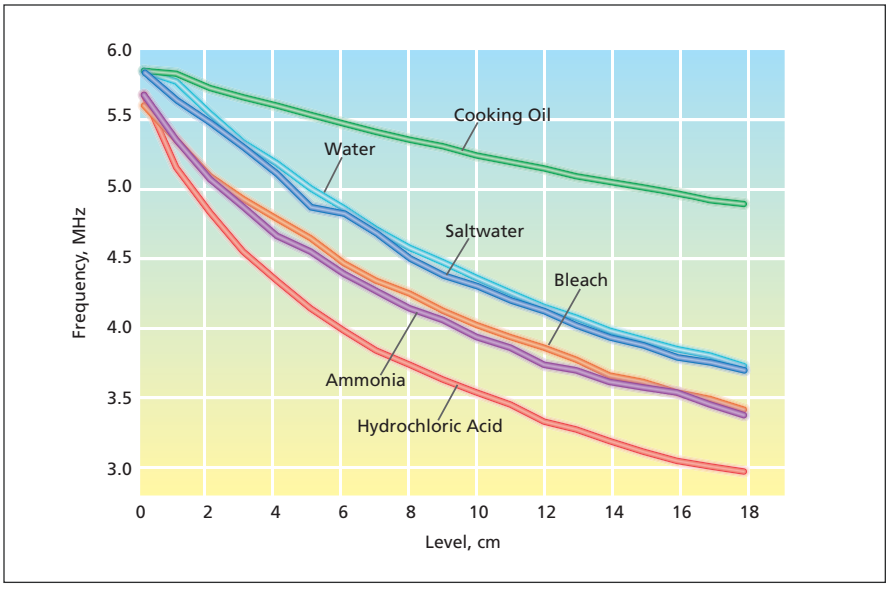

Figure 2. **Resonance Frequency vs. Liquid Level** was measured in experiments in which the sensor of Figure 1 was immersed in several different liquids.

measuring the levels of any fluids that can be stored in electrically nonconductive reservoirs. The sensors can readily be designed and built to withstand cryogenic, acidic, or caustic fluids: The sensor design and the method of powering and interrogating them makes it possible to completely encase the sensors in materials that can be chosen for their ability to endure, and to protect the sensor circuitry against, the harsh fluid environments.

A fluid-level sensor of this type contains a passive resonant circuit comprising an inductor and a pair of parallel capacitor plates, all encased in a material that protects them from the fluid environment (see Figure 1). When the sensor is mounted so that the parallel capacitor plates extend downward into a dielectric fluid, the capacitance increases, and thus resonance frequency of the circuit decreases, as the level of the liquid rises.

The sensor is interrogated by use of the system described in "Magnetic-Field-Response Measurement-Acquisition System" (LAR-16908), *NASA Tech Briefs*, Vol. 30, No. 6 (June 2006) page 28. To recapitulate: The system includes a transmitting/receiving antenna that is placed in proximity to the inductor. The system generates a series of increasing oscillating magnetic field harmonics that powers the sensors. Once powered, the sensors respond with their own oscillating magnetic fields. The system measures the response of the sensor circuitry to excitations at different frequencies to identify the resonance frequency. Hence, once calibration data of liquid level versus resonance frequency have been acquired (see Figure 2), the sensor can be used as a fluid-level sensor.

This work was done by Stanley E. Woodard of Langley Research Center and Bryant D. Taylor of Swales Aerospace. Further information is contained in a TSP (see page 1). LAR-17155

Interference-Detection Module in a Digital Radar Receiver

This concept applies to receivers in consumer electronic devices and automotive radar systems.

NASA's Jet Propulsion Laboratory, Pasadena, California

A digital receiver in a 1.26-GHz spaceborne radar scatterometer now undergoing development includes a module for detecting radio-frequency interference (RFI) that could contam-inate scientific data intended to be acquired by the scatterometer. The role of the RFI-detection module is to identify time intervals during which the received signal is likely to be contaminated by RFI and thereby to enable exclusion, from further scientific data processing, of signal data acquired during those intervals. The underlying concepts of detection of RFI and rejection of RFI-contaminated signal data are also potentially applicable in advanced terrestrial radio receivers, including software-defined radio receivers in general, receivers in cellular telephones and other wireless consumer electronic devices, and receivers in automotive collision-avoidance radar systems.

The improvement afforded by the present RFI module is best seen against the background of prior scatterometer back-end receiver designs. It has been conventional practice to either (1) use analog square-law detection and integration at an intermediate frequency (IF) or (2) sample an echo having a bandwidth of no more than hundreds of kilohertz at baseband and then perform Fourier-transform and magnitude-squared calculations in digital processing. Both of these conventional practices provide accurate estimates of total received power, but they also destroy, through averaging, information on the signal statistics (especially, the voltage probability distribution) in each echo measurement. This is unfortunate because the statistical information can serve as an indication of whether the scatterometer is receiving only the desired reflections from a distributed natural target or is receiving interfering signals from artificial sources in addition to, or instead of, the desired reflections.

The RFI-detection module is part of a digital square-law scatterometer processor (SP) implemented in a field-programmable gate array (FPGA). The raw scatterometer output signal used to generate an input signal for the SP is a down-converted signal at offset video frequencies in the range from 2 to 6 MHz. This signal is alternated in time with either radar echo pulses or a receiver "noise-only" measurement signal. The video signal is processed by an analog-to-digital converter (ADC) at a sampling rate of 16 MHz (greater than the Nyquist sampling rate) before being sent to the SP FPGA. The main part of the SP calculates the signal power by use of square-and-accumulate logic during each successive receiving time window. At the same time, raw magnitude (absolute-value) information from the ADC is fed to the RFI-detection module at the full 16-MHz sampling rate.

The RFI-detection module (see figure) compares raw data samples to a pair of register values that can be programmed to set the sensitivity of an RFI-detection algorithm. The first register value defines an amplitude threshold for counting a radar return sample as being "strong." The second register value defines a "count-exceed" value for strong samples: if this value is exceeded during a given time window, an RFI flag for that time window is triggered. In effect, the RFI-detection module performs a coarse calculation of the probability density function of the received signal by gauging whether there are many outliers in an otherwise weak signal. Because the accounting is done at the full 16-MHz Nyquist sampling rate, temporal information is preserved in the algorithm down to the time scale of one sample (62.5 ns).

Gate signals that delineate the successive processing windows are sent from a separate FPGA radar-control-and-timing unit. The signal-power values calculated by the SP are sent to a buffer memory. At the beginning of a time window, a 12-bit down counter is loaded with the "count-exceed" value. During the window, the absolute-value sample data are compared with the RFI amplitude threshold register value. If a sample equals or exceeds the threshold, it is deemed to be an RFI-contaminated sample, and the 12-bit down-counter is decremented. If the down-counter reaches a value of zero before the end of the window, then the RFI flag is set, and buffered data for this window are labeled accordingly to tprevent further processing. The flag is cleared at the beginning of the next window.

For an electrically quiet scene, the noise-only voltage measurement yields a low-level Gaussian-distributed thermal noise signal (receiver noise plus the an-

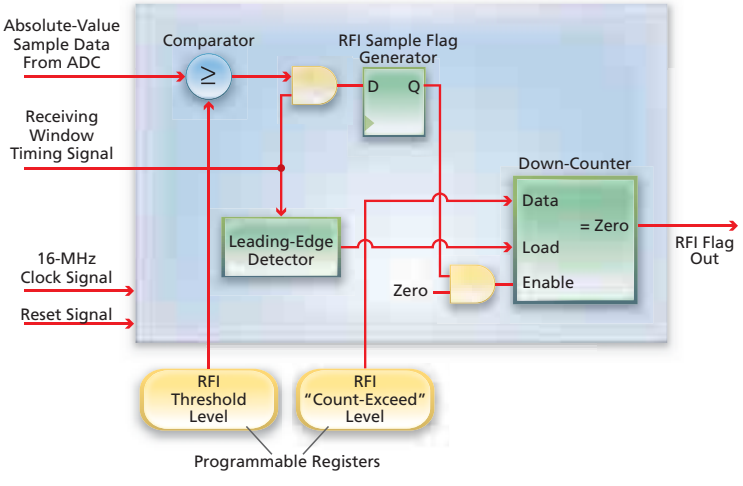

The **RFI-Detection Module** generates a flag signal indicating RFI when a signal exceeds a preset threshold value on more than a preset number of occasions during each successive receiving time window.

tenna brightness temperature). If RFI is present in sufficient strength, it contributes a coherent signal component that spreads the probability density function of the signal in such a manner as to cause the signal to be flagged by the RFI-detection module in the SP. It has been estimated that in the original intended spaceborne-radar-scatterometer application, the effects of RFI could be effectively mitigated by commanding the SP to detect peak power levels about 10 dB above the thermal noise floor of the radar receiver.

This work was done by Mark Fischman, Andrew Berkun, Anhua Chu, Adam Freedman, Michael Jourdan, Dalia McWatters, and Mimi Paller of Caltech for NASA's Jet Propulsion Laboratory. Further information is contained in a TSP (see page 1).

In accordance with Public Law 96-517, the contractor has elected to retain title to this invention. Inquiries concerning rights for its commercial use should be addressed to:

Innovative Technology Assets Management
JPL
Mail Stop 202-233
4800 Oak Grove Drive
Pasadena, CA 91109-8099
E-mail: iaoffice@jpl.nasa.gov

Refer to NPO-45045, volume and number of this NASA Tech Briefs *issue, and the page number.*

Modal Vibration Analysis of Large Castings

Massive objects can be tested *in situ*, without precisely controlling boundary conditions.

John F. Kennedy Space Center, Florida

The art of experimental modal vibration analysis (MVA) has been extended to apply to large castings. This extension was made to enable the use of experimental MVA as a relatively inexpensive, simple means of assessing the internal structural integrity of tread shoes of crawler transporters used to move spacecraft to the launch pad at Kennedy Space Center. Each tread shoe is made from cast iron and weighs about a ton (has a mass ≈907 kg). The present extended version of experimental MVA could also be applied to other large castings. It could be especially useful to manufacturers as a means of rapidly discriminating against large castings that contain unacceptably large concentrations of internal defects.

The use of experimental MVA to assess structural integrity is not new. What are new here are those aspects of the extension of experimental MVA that pertain to the application of MVA to objects so massive that it may not be practical or cost effective to mount them in special test fixtures that impose special test boundary conditions to test them in place under normal conditions of use.

Some background information on experimental MVA is prerequisite to a meaningful description of the extension of experimental MVA to crawler tread shoes and similar large castings. In experimental MVA, one measures the vibrational response of a structural component to an impulse and/or to a continuous vibrational excitation. The measurement data are processed to obtain modal parameters that characterize the response: these parameters include modal frequencies [resonance (natural) frequencies of vibrational modes], mode-shape parameters, and modal damping parameters. The structural response as thus characterized is a unique signature that is a function of the geometry and the characteristics of the material (mass density and moduli of elasticity and rigidity, among others) of the component. Structural flaws, which are significant, show as changes to this modal signature. This concludes the background information.

The **Setup for Experimental MVA** on a massive crawler tread shoe is simple and can be implemented easily: The placements of the modal-hammer blow and accelerometer are not critical.

In experimental MVA of a crawler tread shoe or a similar large object, one excites vibrations by use of an instrumented modal hammer, which is a hammer designed for use in experimental MVA and, more specifically, to apply an impulsive force of sufficient magnitude for a sufficiently short time to excite all of the vibrational modes within a wide frequency range of interest. The vibrational response is measured by use of an accelerometer mounted on the shoe (see figure). The modes of greatest significance for assessment of the structural integrity of the shoe are first three or four bending modes and an axial mode (typically, the first one).

In experimental MVA in general, the natural frequencies are global properties of the structural component under test and manifest themselves as peaks in the frequency spectra of the responses of the component. In the case of a crawler tread or other casting, a crack, void, slag inclusion, or porosity reduces stiffness in a global sense, reducing the natural frequencies of one or more modes. Such reductions in natural frequency are measurable and are useful for assessing structural integrity, operational safety, and reliability.

Data from finite-element analysis and experiments on the crawler tread shoes confirm the experimental modal results showing that the tread shoes are relatively insensitive to boundary conditions, such that experimental MVA *in situ*, without modifications to control boundary conditions, can be used to assess the structural integrity of the shoes. More specifically, the results have been found to be largely insensitive to the locations of the hammer hit and the accelerometer location and to be repeatable after crawler motion and after changes in tension applied by pins that hold the shoes in place.

This work was done by Rudolph J. Werlink and Ravi N. Margasahayam of Kennedy Space Center. Further information is contained in a TSP (see page 1). *KSC-13155*

Structural/Radiation-Shielding Epoxies

Pendant aliphatic groups are incorporated as integral parts of molecular structures.

Langley Research Center, Hampton, Virginia

A development effort was directed toward formulating epoxy resins that are useful both as structural materials and as shielding against heavy-ion radiation. Hydrogen is recognized as the best element for absorbing heavy-ion radiation, and high-hydrogen-content polymers are now in use as shielding materials. However, high-hydrogen-content polymers (e.g. polyethylene) are typically not good structural materials. In contrast, aromatic polymers, which contain smaller amounts of hydrogen, often have the strength necessary for structural materials. Accordingly, the present development effort is based on the concept that an ideal structural/heavy-ion-radiation-shielding material would be a polymer that contains sufficient hydrogen (e.g., in the form of aliphatic molecular groups) for radiation shielding and has sufficient aromatic content for structural integrity.

As part of this development, an aromatic/ aliphatic diamine (see Figure 1) was prepared for incorporation into structural-epoxy formulations. The diamine reacts with the epoxy in the same manner as the ones in conventional structural epoxy systems giving a crosslinked network. The aliphatic portions of the diamine molecules are covalently attached to the aromatic portions in a pendant fashion and are not involved in the crosslinking molecular network. Thus, aliphatic content is introduced without negatively affecting mechanical properties. In addition, the aliphatic chains cannot leach out, as sometimes happens in formulations that include hydrogen-bearing molecules as additives.

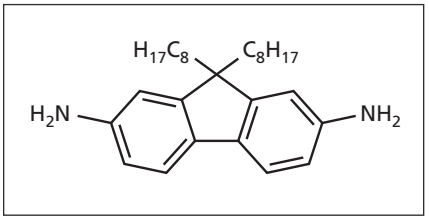

Figure 1. This **Aromatic/Aliphatic Diamine** was included in epoxy formulations as a means of incorporating high permanent hydrogen content without excessively compromising strength and stiffness.

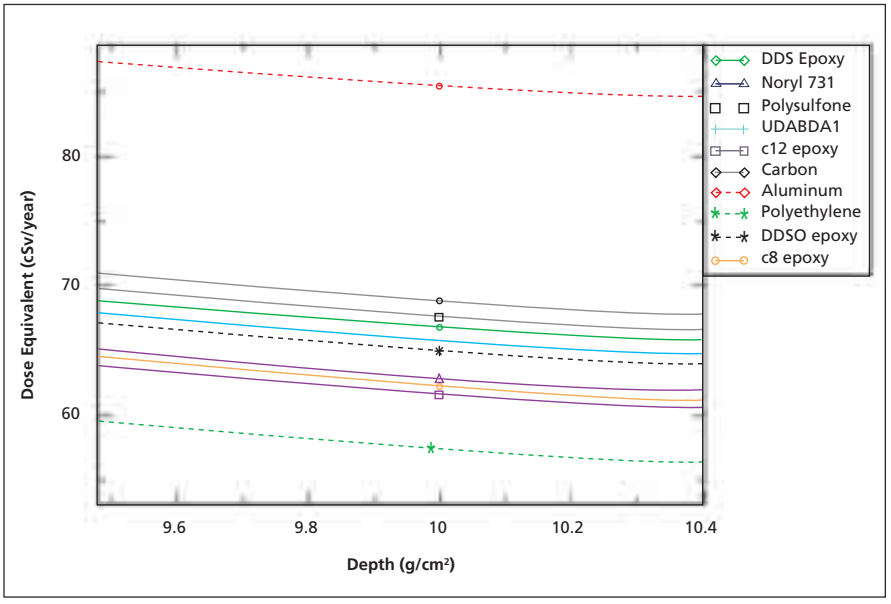

Figure 2. **HZETRN Modeling** is shown for various materials.

In a typical reaction, the aromatic/aliphatic diamine was slowly added to tetraglycidyl methylene dianiline (an epoxy) while heating to a temperature of 60 °C in a stainless steel mold. The mixture was subsequently heated to 80 °C under vacuum, then placed in a conventional oven and heated to 100 °C for 14 h, 120 °C for 1 h, 140 °C for 1 h, and 177 °C for 1 h to complete the cure.

The predicted radiation-shielding properties of two variants of this epoxy, were compared to those of polyethylene, aluminum, carbon, and other structural materials including a conventional structural epoxy system (DDSO epoxy) using a well-tested NASA radiation-transport computer code known as HZETRN (Figure 2). The radiation-shielding properties of the two variants of this epoxy, c8 and c12 in Figure 2, were the closest to those of polyethylene.

Mechanical tests were performed on samples of this epoxy to determine its potential as a structural material. The average compressive modulus and the apparent compressive strength from four specimens were 2.86 ± 0.19 GPa and 52.5 ± 3.7 MPa, respectively. The compressive modulus is nearly equal to that of a typical untoughened tetrafunctional aerospace epoxy resin. The compressive strength should be regarded as a lower bound because specimens in these tests were too thin and did not fail in pure compression, and chips on their edges initiated brittle failures.

This work was done by John W. Connell, Joseph G. Smith, Jeffrey Hinkley, and Steve Blattnig of Langley Research Center; Donavon M. Delozier and Kent A. Watson of the National Institute of Aerospace; and Sayata Ghose of the Oak Ridge Associated Universities. Further information is contained in a TSP (see page 1).

This invention is owned by NASA, and a patent application has been filed. Inquiries concerning nonexclusive or exclusive license for its commercial development should be addressed to the Patent Counsel, Langley Research Center, at (757) 864-3521. Refer to LAR-16874-1.

Integrated Multilayer Insulation

IMLI offers several potential advantages over conventional MLI.

John H. Glenn Research Center, Cleveland, Ohio

Integrated multilayer insulation (IMLI) is being developed as an improved alternative to conventional multilayer insulation (MLI), which is more than 50 years old. A typical conventional MLI blanket comprises between 10 and 120 metallized polymer films separated by polyester nets. MLI is the best thermal-insulation material for use in a vacuum, and is the insulation material of choice for spacecraft and cryogenic systems. However, conventional MLI has several disadvantages: It is difficult or impossible to maintain the desired value of gap distance between the film layers (and consequently, it is difficult or impossible to ensure consistent performance), and fabrication and installation are labor-intensive and difficult. The development of IMLI is intended to overcome these disadvantages to some extent and to offer some additional advantages over conventional MLI.

The main difference between IMLI and conventional MLI lies in the method of maintaining the gaps between the film layers. In IMLI, the film layers are separated by what its developers call a micro-molded discrete matrix, which can be loosely characterized as consisting of arrays of highly engineered, small, lightweight, polymer (typically, thermoplastic) frames attached to, and placed between, the film layers (see Figure 1). The term "micro-molded" refers to both the smallness of the frames and the fact that they are fabricated in a process that forms precise small features, described below, that are essential to attainment of the desired properties. The term "discrete" refers to the nature of the matrix as consisting of separate frames, in contradistinction to a unitary frame spanning entire volume of an insulation blanket.

Figure 1. In this **Prototype Assembly**, a discrete matrix comprising a square array of square frames is placed on a metallized polymer film. In constructing a multilayer insulation blanket, arrays like this one would be placed between all the metallized polymer film layers.

Figure 2 depicts selected aspects of a frame according to one design concept. The frame would consist of posts and beams. Assembly would be relatively easy. The ends of the posts would mate with holes in the film layers. Posts in successive frame layers would be joined end-to-end by snap joints that would be molded as integral parts of the posts. The desired separation distance between film layers would be maintained consistently because the film layers would be clamped between adjoining posts at the snap joints. The snap joints would have features that would make it easy to snap the posts together and impossible to snap apart. The posts and frames would maintain sufficient gaps for outgassing. For a terrestrial application in which it is required to evacuate the interior spaces, the posts could also support an outer metal layer that would serve as a vacuum shell.

Because the distance between layers could be maintained consistently, it would be possible to optimize this distance and the concomitant dimensions of the frames to provide the necessary structural support while minimizing the contact area and the associated conductive heat leak through the frame. Thus,

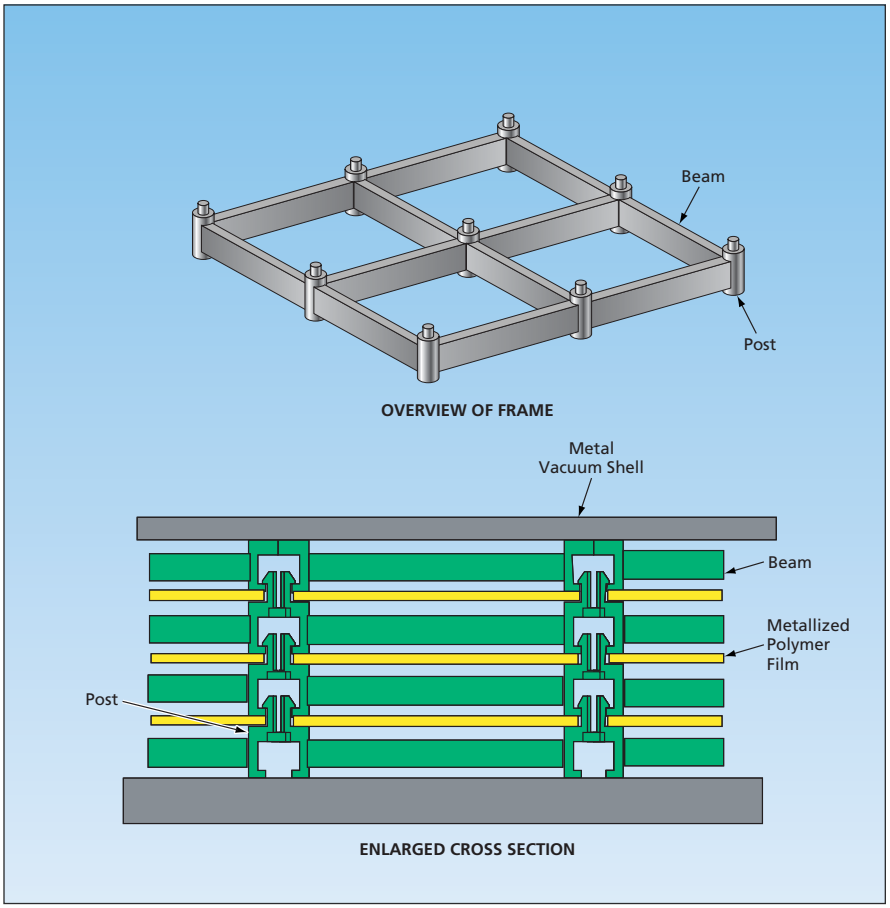

Figure 2. **Post-and-Beam Frames** would be molded as integral units. Posts in each layer would be joined end-to-end with posts in the next layer by means of integral snap joints.

relative to conventional MLI, IMLI would be a more highly engineered system. The matrix spacer is designed to reduce heat conduction to minimum levels, and the multiple radiation shields reduce radiative heat leak, so that the entire insulation system is near the radiation limit. Thermal modeling indicated IMLI should have a thermal conductivity 63% that of conventional MLI. It has been estimated that in a typical application, the mass of an IMLI panel with a vacuum shell would be approximately one-third that of an equivalent conventional MLI with a vacuum shell. Phase II work in progress has developed a second generation IMLI system with a calculated heat leak of 0.139 W/m^2 ($e^* = 0.000325$) for a 40-layer blanket, which is less than half the heat leak of traditional MLI.

This work was done by Scott Dye of Quest Product Development Corp. for Glenn Research Center.

Inquiries concerning rights for the commercial use of this invention should be addressed to NASA Glenn Research Center, Innovative Partnerships Office, Attn: Steve Fedor, Mail Stop 4–8, 21000 Brookpark Road, Cleveland, Ohio 44135. Refer to LEW-18270-1/1-1.

Apparatus for Screening Multiple Oxygen-Reduction Catalysts

Multiple specimens are tested simultaneously at equal potential in the same solution.

NASA's Jet Propulsion Laboratory, Pasadena, California

An apparatus that includes an array of multiple electrodes has been invented as a means of simultaneously testing multiple materials for their utility as oxygen-reduction catalysts in fuel cells. The apparatus ensures comparability of test results by exposing all the catalyst-material specimens to the same electrolytic test solution at the same potential. Heretofore, it has been possible to test only one specimen at a time, using a precise rotating disk electrode that provides a controlled flux of solution to the surface of the specimen.

For each set of catalytic materials to be tested, the electrodes and their current collectors (see figure) are fabricated as gold-film patterns on a flexible poly(vinylidene fluoride) substrate that is typically a fraction of a millimeter thick. The electrode areas measure 5 by 5 mm. The electrode areas are coated with thin films of the catalytic materials to be tested. The chemical compositions of these films are established in a combinatorial deposition process: The films are sputter-deposited simultaneously onto all the electrodes from targets made of different materials at different positions relative to the array. Hence, the composition of the deposit on each electrode is unique, dependent on its position. The composition gradient across the area of the array and, hence, the variations among compositions of deposits on the electrodes, can be tailored by adjusting the target/substrate geometry and the relative target powers.

The resulting flexible electrode fixture is placed on the inside wall of a 20-cm-diameter vertical cylindrical container with the electrodes facing inward. The current collectors are connected to the input terminals of a multichannel potentiostat. The container is filled with electrolyte solution. In operation, oxygen is bubbled through the solution and the solution is stirred rapidly (e.g., by use of a conventional propeller/impeller or a magnetic stirrer) to maintain a laminar flow of consistently oxygenated solution over the electrodes. During operation, the multichannel potentiostat simultaneously measures the currents generated at all the electrodes as functions of an applied bias voltage. Typically, the voltage is varied in a slow potentiodynamic scan.

This work was done by Jay Whitacre and Sekharipuram Narayanan of Caltech for NASA's Jet Propulsion Laboratory. Further information is contained in a TSP (see page 1).

In accordance with Public Law 96-517, the contractor has elected to retain title to this invention. Inquiries concerning rights for its commercial use should be addressed to:

Innovative Technology Assets Management
JPL
Mail Stop 202-233
4800 Oak Grove Drive
Pasadena, CA 91109-8099
(818) 354-2240
E-mail: iaoffice@jpl.nasa.gov

Refer to NPO-43220, volume and number of this NASA Tech Briefs *issue, and the page number.*

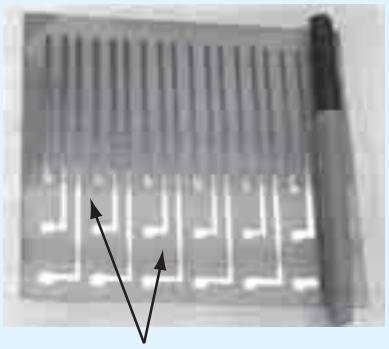

This **Array of Eighteen Gold Electrodes** and current collectors was fabricated on a 0.5-mm-thick PVDF sheet. Each electrode is coated with a different catalytic material to be tested.

Determining Aliasing in Isolated Signal Conditioning Modules

Input anti-aliasing filters eliminate rogue frequencies that cause aliasing.

Dataforth Corporation, Tucson, Arizona

Within a digital world, the parameters of real-world information (temperature, voltage, current, speed, flow, pressure, distance, etc.) used for process communications and control are analog in nature. Processing this information is achieved primarily using digital signal processing techniques. The age of microelectronics has made it possible for digital processing power to be extended into the field where sensors are located; thus, much preprocessing can be accomplished outside the main computer or PC.

There are many issues that can create serious problems along the way, such as EMI noise, grounding, accuracy, resolution, aging, drift, isolation, and noisy power supplies. In addition, there is one very subtle problem that often goes unnoticed but can lurk in the background. Known as aliasing, this problem exists in isolated signal conditioning modules (SCMs) and anywhere an analog-to-digital converter is active.

The basic concept of aliasing is this: Converting analog data into digital data requires sampling the signal at a specific rate, known as the sampling frequency. The result of this conversion process is a new function, which is a sequence of digital samples. This new function has a frequency spectrum, which contains all the frequency com-

ponents of the original signal. The Fourier transform mathematics of this process show that the frequency spectrum of the sequence of digital samples consists of the original signal's frequency spectrum plus the spectrum shifted by all the harmonics of the sampling frequency. If the original analog signal is sampled in the conversion process at a minimum of twice the highest frequency component contained in the analog signal, and if the reconstruction process is limited to the highest frequency of the original signal, then the reconstructed signal accurately duplicates the original analog signal. It is this process that can give birth to aliasing.

To illustrate, consider a time function signal consisting of two sinusoids, one at 25 Hz, and the other expected to be at 180 Hz. This sampling process uses a sampling frequency of 400 Hz (which is greater than 2*180 Hz) and the reconstruction process has a bandwidth limit of 200 Hz. The only frequency components that will appear in the conversion are 25 Hz and 180 Hz. However, if the original signal's highest frequency is not the expected 180 Hz but 213 Hz, a reconstructed signal consisting of 25 Hz and 187 Hz (400-213) will result. The 213-Hz signal component appears in the output as the 187-Hz component (187 Hz "alias" 213 Hz).

Since all signal conditioning modules that provide isolation typically use some form of analog sampling conversion process to move analog information across an isolation barrier, it is critical for system engineers to examine their application carefully to determine whether aliasing can occur.

This work was done by Dataforth Corporation. For more information, visit ***http://info.hotims.com/22914-122.***

Composite Bipolar Plate for Unitized Fuel Cell/Electrolyzer Systems

A weight-saving design is applicable toward space missions, submarines, and high-altitude aircraft.

John H. Glenn Research Center, Cleveland, Ohio

In a substantial improvement over present alkaline systems, an advanced hybrid bipolar plate for a unitized fuel cell/electrolyzer has been developed. This design, which operates on pure feed streams (H_2/O_2 and water, respectively) consists of a porous metallic foil filled with a polymer that has very high water transport properties. Combined with a second metallic plate, the pore-filled metallic plates form a bipolar plate with an empty cavity in the center.

In electrolyzer mode, this cavity fills with water, which cools the stack, and provides the water for the electrolysis. The water passes through the polymer-filled pores under an RH gradient and feeds the electrolysis reaction. Under fuel-cell mode, the water is vacuumed out of the chamber with vacuum being continuously applied to remove water from the fuel-cell reaction. This evaporative cooling also provides heat removal from the stack.

At 80 °C, electrolyzer performance was superior to that of flowing water in the hydrogen chamber up to 400 mA/cm^2. Above this current density, the membrane begins to dry out as water cannot be carried to the oxygen electrode fast enough. Similar behavior was seen when operating under fuel-cell mode. The current invention outperformed the traditional flow-through fuel cell up to 300 mA/cm^2. Above this current density, the oxygen chamber begins to flood.

When operating in electrolyzer mode, the hybrid plate generates H_2 and O_2 at much lower water contents than traditional electrolysis cells. This greatly simplifies drying of the product gases. Because the water is the only product from the reaction, the feed gases can be operated under "dead-ended" conditions; thus, eliminating the need for saturation, recirculation, and water/gas separation systems for fuel-cell operation. In both fuel-cell and electrolyzer mode, this advanced, unitized cell shows equal or superior performance to discreet systems. This design also allows for simple high-pressure operation with a high differential pressure.

Keeping all feed reactants and products in the vapor phase leads to a system simplification. This eliminates the biggest challenge to unitized systems (water management), allowing the weight savings of a second stack. A study has been carried out and has successfully demonstrated proof-of-concept. More design work has to be done to translate this concept into a full system.

This work was done by Cortney K. Mittelsteadt and William Braff of Giner Electrochemical Systems, LLC for Glenn Research Center.

Inquiries concerning rights for the commercial use of this invention should be addressed to NASA Glenn Research Center, Innovative Partnerships Office, Attn: Steve Fedor, Mail Stop 4–8, 21000 Brookpark Road, Cleveland, Ohio 44135. Refer to LEW-18269-1.

Spectrum Analyzers Incorporating Tunable WGM Resonators

Resolutions would be much greater than those of current spectrum analyzers.

NASA's Jet Propulsion Laboratory, Pasadena, California

A photonic instrument is proposed to boost the resolution for ultraviolet/optical/infrared spectral analysis and spectral imaging allowing the detection of narrow (0.00007-to-0.07-picometer wavelength resolution range) optical spectral signatures of chemical elements in space and planetary atmospheres. The idea underlying the proposal is to exploit the advantageous spectral characteristics of whispering-gallery-mode (WGM) resonators to obtain spectral resolutions at least three orders of magnitude greater than those of optical spectrum analyzers now in use. Such high resolutions would enable measurement of spectral features that could not be resolved by prior instruments.

Tunable single-mode WGM resonators would be incorporated into optical spectrum analyzers as shown in the block diagram in Figure 1. The center of the spectral window of the spectrum analyzer will be tuned to the carrier frequency of interest. The rough snapshot of the signal under study will be taken. After that, the WGM filter will be inserted in front of the spectrum analyzer. The internal scanning of the spectrum analyzer will be switched off, while the WGM filter will be scanned through the frequency window. The narrow-band spectral features of the signal will be resolved as the result. In particular, for the purpose of measuring abundances of selected isotopes (e.g., isotopes of carbon) in compounds in outer space and in atmospheres of Earth and other planets, an instrument equipped according to the proposal could measure narrow (width < 10 MHz) optical spectral signatures of compounds (e.g., CO_2) containing such isotopes.

The advantageous spectral characteristics of WGM resonators include high resonance quality factors (see Figure 2) and clean spectra. In addition, relative to other tunable optical resonators that have similar free spectral ranges and Q values, tunable single-mode WGM resonators can be tuned over wider frequency bands and exhibit much greater rejection ratios. A tunable single-mode WGM resonator incorporated into a spectrum analyzer according to the proposal would have a power consumption of no more than a few milliwatts, would have a mass of about 100 g, would have no moving parts, and could be operated autonomously. In addition to being key components of contemplated new high-resolution optical spectrum analyzers, tunable single-mode WGM resonators could be retrofit to current optical spectrum analyzers to improve their performances.

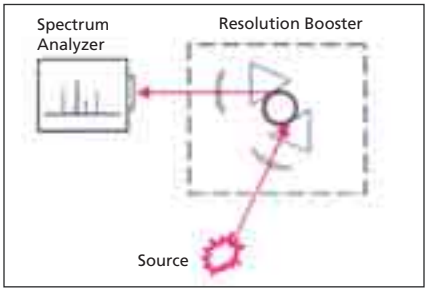

Figure 1. A **Resolution Booster** exploits the advantage of WGM resonators to increase spectral resolution at least three orders of magnitude.

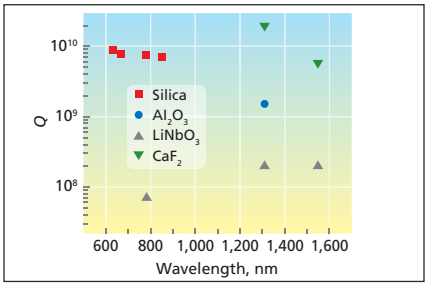

Figure 2. **These Resonance Quality Factors** (Q values) plotted versus wavelength were obtained from measurements on WGM resonators made of the indicated materials.

This work was done by Anatoliy Savchenkov, Andrey Matsko, Dmitry Strekalov, and Lute Maleki of Caltech for NASA's Jet Propulsion Laboratory. Further information is contained in a TSP (see page 1).

In accordance with Public Law 96-517, the contractor has elected to retain title to this invention. Inquiries concerning rights for its commercial use should be addressed to:

Innovative Technology Assets Management
JPL
Mail Stop 202-233
4800 Oak Grove Drive
Pasadena, CA 91109-8099
(818) 354-2240
E-mail: iaoffice@jpl.nasa.gov

Refer to NPO-43993, volume and number of this NASA Tech Briefs *issue, and the page number.*

Quantum-Well Thermophotovoltaic Cells

Conversion efficiencies more than twice those of prior thermophotovoltaic cells are expected.

Marshall Space Flight Center, Alabama

Thermophotovoltaic cells containing multiple quantum wells have been invented as improved means of conversion of thermal to electrical energy. The semiconductor bandgaps of the quantum wells can be tailored to be narrower than those of prior thermophotovoltaic cells, thereby enabling the cells to convert energy from longer-wavelength photons that dominate the infrared-rich spectra of typical thermal sources with which these cells would be used. Moreover, in comparison with a conventional single-junction thermophotovoltaic cell, a cell containing multiple narrow-bandgap quantum wells according to the invention can convert energy from a wider range of wavelengths. Hence, the invention increases the achievable thermal-to-electrical energy-conversion efficiency. These thermophotovoltaic cells are expected to be especially useful for extracting electrical energy from combustion, waste-heat, and nuclear sources having temperatures in the approximate range from 1,000 to 1,500 °C.

In its original form, the invention applies to the $In_xGa_{1-x}As$ ($0<x<1$)-and-InP material system. In principle, it is equally applicable to any narrow-bandgap semiconductor material system that is amenable to the growth of lattice-matched multiple quantum wells on suitable substrates. A cell according to the invention is best described with reference to the corresponding conventional $In_xGa_{1-x}As$ thermophotovoltaic cell, which is an electron-acceptor-doped/intrinsic/electron-donor-doped (p/i/n) $In_{0.47}Ga_{0.53}As$ cell lattice-matched to an InP substrate. In the cell according to the invention, instead of the intrinsic (undoped) region, there are multiple strained, lattice-matched, narrow-bandgap quantum wells comprising layers of $In_xGa_{1-x}As$ ($x>0.6$) interspersed with layers of $In_{0.47}Ga_{0.53}As$. It has been estimated that for black-body thermal sources having temperatures between 1,000 and 1,500 °C, the energy-conversion efficiencies of thermophotovoltaic cells according to the invention can be more than twice those of the corresponding conventional $In_xGa_{1-x}As$ thermophotovoltaic cells.

An appropriate choice of the number of quantum wells and the thicknesses of the individual quantum-well layers (typically of the order of a few nanometers) in conjunction with the selection of the quantum-well materials makes it possible to prevent the generation of lattice-mismatch crystal defects in the quantum-well layers. Thus, it is possible to prevent the degradation of crystalline quality and thereby prevent the consequent degradation of electronic performance associated with the fabrication of thicker conventional lattice-mis-

matched devices. Inasmuch as conventional $In_xGa_{1-x}As$ thermophotovoltaic cells are already manufactured by techniques compatible with the growth of multiple quantum wells, little additional expense would be incurred by adding quantum-well-growth steps to conventional manufacturing processes.

This work was done by Alex Freudlich and Alex Ignatiev of the University of Houston for Marshall Space Flight Center. For more information, contact Sammy Nabors, MSFC Commercialization Assistance Lead, at sammy.a.nabors@nasa.gov. Refer to MFS-32545-1

Bounded-Angle Iterative Decoding of LDPC Codes

Maximum undetected-error rates are reduced greatly; overall error rates are increased negligibly (at low error rates).

NASA's Jet Propulsion Laboratory, Pasadena, California

Bounded-angle iterative decoding is a modified version of conventional iterative decoding, conceived as a means of reducing undetected-error rates for short low-density parity-check (LDPC) codes. For a given code, bounded-angle iterative decoding can be implemented by means of a simple modification of the decoder algorithm, without redesigning the code.

Iterative decoders for well-designed LDPC codes are inherently capable of detecting as well as correcting errors. In a given instance, an error is detected if a code word is not found at the conclusion of iterations: that is, an error is detected if the estimated code symbols at the end of iterations do not constitute a valid code word. However, when this approach is followed without modification, the maximum undetected-error rates obtained for short LDPC codes are typically too high for many applications.

Bounded-angle iterative decoding is based on a representation of received words and code words as vectors in an n-dimensional Euclidean space (where n is an integer). In bounded-angle iterative decoding as in conventional iterative decoding, the estimates of the decoder are rejected (an error is detected) if a code word is not found before the maximum allowed number of iterations. Conversely, iterations may be stopped as soon as a code word is detected. The difference between bounded-angle and conventional iterative decoding manifests itself once a code word has been detected. At this point, the decoding algorithm computes the angle in the n-dimensional Euclidean space between the received word and the detected code word. If this angle is less than an arbitrarily specified threshold angle, θ_d, then the detected code word is accepted; if this angle exceeds θ_d, then the detected code word is rejected.

The undetected-error rate in bounded-angle iterative decoding is necessarily less than that in conventional iterative decoding because the modified decoding algorithm rejects at least the same code words as does the conventional decoding algorithm. By rejecting more code words, the modified algorithm reduces the undetected-error rate while increasing the overall error rate. Through judicious choice of θ_d, optimized as a function of signal-to-noise ratio E_b/N_0 (see figure), one can reduce the decoder's maximum undetected-error rate by orders of magnitude while increasing its overall error rate by amounts that are negligible for all values of E_b/N_0 high enough to have produced a low error rate using the unmodified decoder. The main value of the modified algorithm lies in the possibility of making this favorable tradeoff between the two error rates, while not redesigning the code and only trivially modifying the decoder.

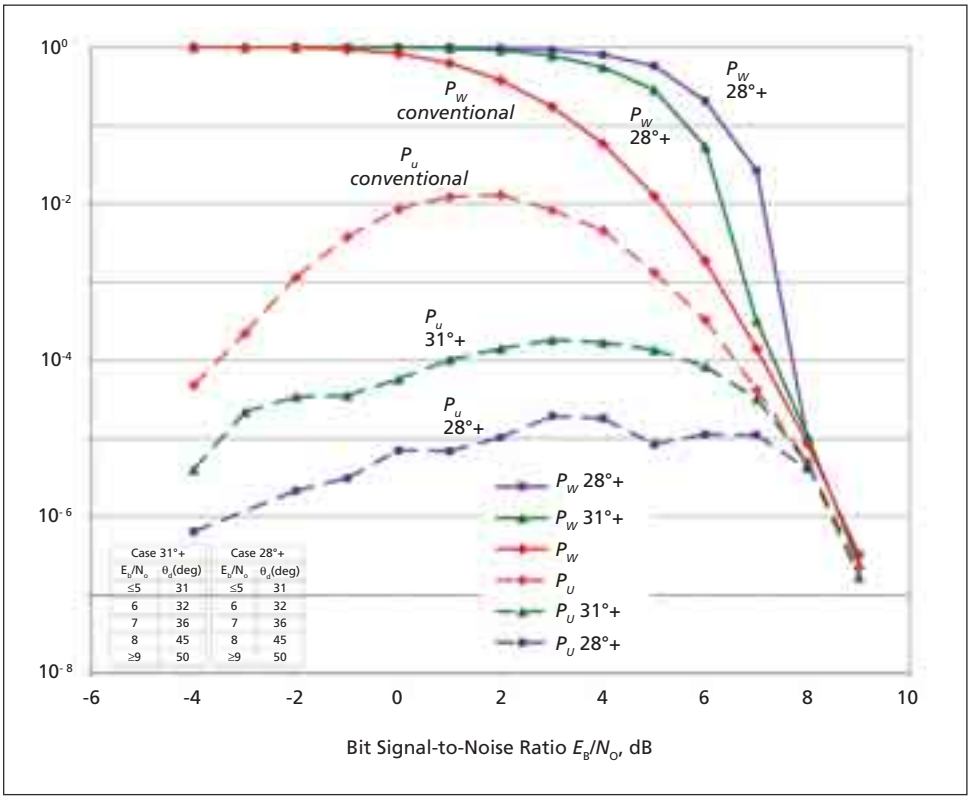

Error Rates in Iterative Decoding of a (32,16) LPDC code were computed for three test cases: one using a conventional decoding algorithm and two using the bounded-angle version of this algorithm with threshold angles of 28° and higher, and 31° and higher, respectively, varying with E_b/N_0 according to the table.

This work was done by Samuel Dolinar, Kenneth Andrews, Fabrizio Pollara, and Dariush Divsalar of Caltech for NASA's Jet Propulsion Laboratory. Further information is contained in a TSP (see page 1).

In accordance with Public Law 96-517, the contractor has elected to retain title to this invention. Inquiries concerning rights for its commercial use should be addressed to:

Innovative Technology Assets Management
JPL
Mail Stop 202-233
4800 Oak Grove Drive
Pasadena, CA 91109-8099
E-mail: iaoffice@jpl.nasa.gov

Refer to NPO-46003, volume and number of this NASA Tech Briefs *issue, and the page number.*

Conversion From Tree to Graph Representation of Requirements

A complete representation without duplicate nodes is generated automatically.

Goddard Space Flight Center, Greenbelt, Maryland

A procedure and software to implement the procedure have been devised to enable conversion from a tree representation to a graph representation of the requirements governing the development and design of an engineering system. The need for this procedure and software and for other requirements-management tools arises as follows: In systems-engineering circles, it is well known that requirements-management capability improves the likelihood of success in the team-based development of complex systems involving multiple technological disciplines. It is especially desirable to be able to visualize (in order to identify and manage) requirements early in the system-design process, when errors can be corrected most easily and inexpensively.

Heretofore, largely for computational convenience, hierarchies of requirements have been visually represented as trees. However, the tree representation is inadequate because the underlying data structures of sets of requirements are graphs. A complete tree representation of a set of requirements usually involves repetition of some requirements nodes. In a case in which there are only a few requirements, the duplication of requirements nodes is not a significant barrier to complete understanding of relationships in the requirements document. In a typical real-world case involving a large number of requirements, the presence of many duplicate nodes makes it difficult or impossible for designers to be certain that all relationships among requirements have been identified. This leads to decision-making based on an incomplete picture of the role of a given requirement in the design of the overall system. In contrast, the graph representation provides a complete picture of relationships among requirements.

The procedure is embodied in algorithms that, in turn, are implemented in a Java-language computer program called "PaladinRM." The input to the algorithms is an Extensible Markup Language (XML) representation of requirements, generated by a previously developed computer program called "SLATE," that is equivalent to a tree representation. Exploiting portions of a body of work known among software experts as the Resource Description Framework, some of the algorithms first process the input into an equivalent graph data structure that does not contain duplicate nodes. Then a modified version of a previously proposed hierarchical-graph-layout algorithm is used to construct a block diagram equivalent to the graph data structure. The resulting display on the computer screen is a layered, directed graph (see figure) that assists in visualization of the hierarchy of requirements applicable to the system at various levels of abstraction (e.g., system, subsystems, and components).

The display, the algorithms, and the underlying procedure enable enhancement of the management of requirements with the following features:

- Visual representation of a subsection of the requirements document;
- Differential update of the database of requirements, based on the changes made during visual display of the requirements; and
- Annotation of requirement nodes with attributes of interest.

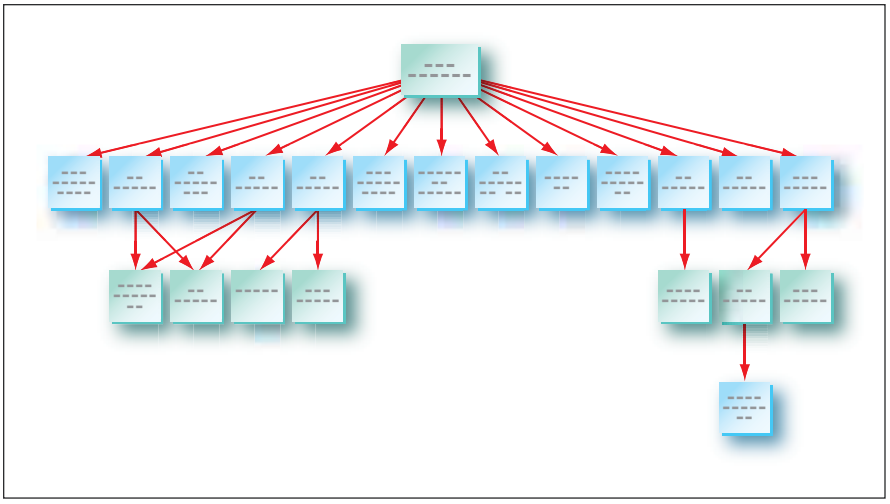

This **Requirement Graph** is a simplified example of the display generated by the procedure summarized in the text.

This work was done by David Frank Everett of Goddard Space Flight Center and Vimal Mayank, Natalya Shmunis, and Mark Austin of the University of Maryland.

In accordance with Public Law 96-517, the contractor has elected to retain title to this invention. Inquiries concerning rights for its commercial use should be addressed to:

University of Maryland
6200 Baltimore Ave., Suite 300
College Park, MD 20742

Refer to GSC-14951-1, volume and number of this NASA Tech Briefs *issue, and the page number.*

Books & Reports

Parallel Hybrid Vehicle Optimal Storage System

A paper reports the results of a Hybrid Diesel Vehicle Project focused on a parallel hybrid configuration suitable for diesel-powered, medium-sized, commercial vehicles commonly used for parcel delivery and shuttle buses, as the missions of these types of vehicles require frequent stops. During these stops, electric hybridization can effectively recover the vehicle's kinetic energy during the deceleration, store it onboard, and then use that energy to assist in the subsequent acceleration.

This innovation is particularly useful with energy storage devices where the state of charge is readily determined by an easily measurable attribute. The ultracapacitor and pressurized hydraulic storage cylinder are good examples of this type. The state of charge, or energy level, is proportional to the voltage of the ultracapacitor and pressure of the hydraulic cylinder. The method is well suited to hybrid vehicle applications where the hybrid power is primarily used during acceleration and deceleration. This method can be executed with limited vehicle state information. Primarily, the only feedback required is the state of charge of the energy storage device, vehicle speed, and operator throttle request.

The Hybrid Booster Drive (HBD) control system has the potential to have similar benefits with modern diesel and non-diesel engines, and when applied to optimized drive trains. It has the potential to deliver equal or better performance than other systems, and may be produced at reduced cost and complexity. Test data are available that show the implementation of the invention during operation of two prototype hybrid electric vehicles.

This work was done by Aaron P. Bloomfield of Bowling Green State University, Electric Vehicle Institute, for Glenn Research Center. Further information is contained in a TSP (see page 1).

Inquiries concerning rights for the commercial use of this invention should be addressed to NASA Glenn Research Center, Innovative Partnerships Office, Attn: Steve Fedor, Mail Stop 4–8, 21000 Brookpark Road, Cleveland, Ohio 44135. Refer to LEW-18289-1.

Anaerobic Digestion in a Flooded Densified Leachbed

A document discusses the adaptation of a patented biomass-digesting process, denoted sequential batch anaerobic composting (SEBAC), to recycling of wastes aboard a spacecraft. In SEBAC, high-solids-content biomass wastes are converted into methane, carbon dioxide, and compost.

SEBAC includes three stages: For stage 1, biomass is placed in a vessel, wherein it is fermented and serves as a leachbed. Stage 1 is started by recycling, from stage 3, of leachate, which wets the bed and inoculates it with microorganisms. After stage 1 has been started, it becomes Stage 2, during which leachate is recycled to keep the bed moist. Stage 2 becomes stage 3 when its leachate is used to start a new stage 1. Leachate is conveyed through the leachbeds by gravity and is conveyed between stages by pumping or gravity, and the beds are not flooded. The spacecraft version of SEBAC incorporates modifications to reduce the sizes of reactors and enable operation in microgravity. The modifications include flooding of the leachbeds, pumping to eliminate reliance on gravity, the use of external liquid/gas separators, and densification of biomass in the leachbeds.

This work was done by David P. Chynoweth, Arthur A. Teixeira, John M. Owens, and Patrick J. Haley of the University of Florida for Johnson Space Center. For further information, contact the JSC Innovation Partnerships Office at (281) 483-3809.

In accordance with Public Law 96-517, the contractor has elected to retain title to this invention. Inquiries concerning rights for its commercial use should be addressed to:

University of Florida
Environmental Systems
Commercial Space Technology Center
AP Black Hall
P.O. Box 116450
Gainesville FL 32611-6450
Phone No.: (352) 392-7814
Fax No.: (352) 392-3673

Refer to MSC-23815-1, volume and number of this NASA Tech Briefs *issue, and the page number.*


NASA
National Aeronautics and
Space Administration